2010

Quantifying Individual Potential Contributions of the Hybrid Sulfur Electrolyzer

John A. Staser
University of South Carolina - Columbia

Maximilian B. Gorensek

John W. Weidner
University of South Carolina - Columbia, weidner@engr.sc.edu

Publication Info

Journal of the Electrochemical Society, 2010, pages B952-B958.

Publisher's link: http://dx.doi.org/10.1149/1.3397901
DOI: 10.1149/1.3397901

Journal of The Electrochemical Society, **157** (6) B952-B958 (2010)
0013-4651/2010/157(6)/B952/7/$28.00 © The Electrochemical Society

Quantifying Individual Potential Contributions of the Hybrid Sulfur Electrolyzer

John A. Staser,[a,c,*,z] Maximilian B. Gorensek,[b] and John W. Weidner[a,*,z]

[a]*Center for Electrochemical Engineering, Department of Chemical Engineering, University of South Carolina, Columbia, South Carolina 29208, USA*
[b]*Computational Sciences Directorate, Savannah River National Laboratory, Aiken, South Carolina 29808, USA*

The hybrid sulfur cycle has been investigated as a means to produce clean hydrogen efficiently on a large scale by first decomposing H_2SO_4 to SO_2, O_2, and H_2O and then electrochemically oxidizing SO_2 back to H_2SO_4 with the cogeneration of H_2. Thus far, it has been determined that the total cell potential for the hybrid sulfur electrolyzer is controlled mainly by water transport in the cell. Water is required at the anode to participate in the oxidation of SO_2 to H_2SO_4 and to hydrate the membrane. In addition, water transport to the anode influences the concentration of the sulfuric acid produced. The resulting sulfuric acid concentration at the anode influences the equilibrium potential of and the reaction kinetics for SO_2 oxidation and the average conductivity of the membrane. A final contribution to the potential loss is the diffusion of SO_2 through the sulfuric acid to the catalyst site. Here, we extend our understanding of water transport to predict the individual contributions to the total cell potential.
 [DOI: 10.1149/1.3397901]

Manuscript submitted November 17, 2009; revised manuscript received March 23, 2010. Published May 3, 2010.

The hybrid sulfur (HyS) cycle has gained attention due to the possibility of using this process to produce clean hydrogen on a large scale at efficiencies higher than those using water electrolysis.[1-19] The high temperature decomposition of H_2SO_4 to SO_2, O_2, and H_2O is suited for use with advanced gas-cooled nuclear reactor heat sources or solar receiver arrays.[1-7] The electrolysis step described here is coupled with the high temperature step to complete the cycle. We developed a gas-fed anode electrolyzer in which SO_2 is oxidized to H_2SO_4 via the following reaction[11,14-18]

$$SO_2+2H_2O \rightarrow H_2SO_4 + 2H^+ + 2e^- \quad U^0_{SO_2} = 0.158 \text{ V vs SHE} \qquad [1]$$

where SHE stands for standard hydrogen electrode. Water required for Reaction 1 is supplied via the membrane from the cathode. H^+ produced in Reaction 1 migrates through the membrane and reduces to hydrogen at the cathode

$$2H^+ + 2e^- \rightarrow H_2 \quad U^0_{H_2} = 0 \text{ V vs SHE} \qquad [2]$$

We have successfully carried out Reactions 1 and 2 over a range of operating conditions (i.e., temperature, flow rate, and membrane pressure differential) and design variations (i.e., catalyst loading and membrane type and thickness).[14-17] We have also accurately predicted water transport and correlated the operating potential to the sulfuric acid concentration produced at the anode.[15-17] We have shown that the concentration of sulfuric acid produced at the anode increases with current density and that the sulfuric acid concentration at the anode influences the cell potential via the reversible cell potential U_{eq}.[18]

Although we have previously correlated cell potential to acid concentration and hence water transport, a quantitative measure of the various potential losses has never been made. In this discussion, we present a comprehensive investigation of the components that make up the total cell potential (i.e., reversible cell potential, membrane resistance, and catalyst activity) to better understand and improve electrolyzer performance and operation.

Experimental

The experimental setup was the same as that described previously.[14-17] The cell was a standard 10 cm^2 cell from Fuel Cell Technologies, Inc. Reactants and products were fed to and from the cell through Kynar manifolds instead of the aluminum endplates. The flow fields were of the standard graphite variety used for fuel cells, which was made possible due to the low cell potentials for SO_2 oxidation. The Kynar/graphite assembly was sandwiched between the aluminum endplates to provide compression, and the temperature was maintained by the use of heating rods inserted into the aluminum endplates.

Liquid water was fed to the cathode by a metering pump and gaseous SO_2 was fed to the anode from a pressure-regulated tank. The cell was maintained at 80°C and the water was heated to 88°C before being fed to the cathode to help maintain the cell temperature. The Nafion (N212 and N115) membrane electrode assembly (MEA) was purchased from Lynntech and had catalyst loadings ranging from 0.5 mg/cm^2 Pt black to 1.5 mg/cm^2 Pt black. The operation of the cells was adjusted so that the conversion of SO_2 was 20%. We have shown previously, however, that conversion and catalyst loading have little effect on the electrolyzer performance.[14] A pressure differential was maintained across the membrane by means of a globe valve at the cathode outlet to control water transport across the membrane.[15]

The membrane specific-area resistance was measured by the current interrupt technique in which the current of the operating electrolyzer was abruptly changed and the transient potential response was monitored. The current interrupt technique was carried out on N212 and N115 membranes tested in the electrolyzer hardware over a range of operating current densities. The hardware resistance was small, less than 0.02 Ω cm^2, and may contribute to the MEA resistance. However, because the hardware resistance was so small, its contribution to the total cell potential has not been investigated independently. The low cell hardware resistance measured for this investigation agreed with the reported values.[20] To confirm the results obtained by the current interrupt technique, Nafion membranes were immersed in sulfuric acid solutions of different concentrations, and the resistance was measured using an ac digital multimeter according to the four-point measurement technique.[21-24]

The resistance of the MEA was measured by hydrogen pump experiments in which hydrogen was oxidized at the anode and reduced at the cathode.[25] The experiment was run such that the membrane was kept hydrated by humidifying the incoming gas streams. The membrane resistance, measured via electrochemical impedance spectroscopy, was subtracted from the MEA resistance to obtain the resistance of the anode and cathode catalyst layers. This value was divided by 2 to yield the resistance of each catalyst layer. The membrane water uptake was measured previously at different sulfuric acid concentrations and different temperatures by equilibrating the membrane in a sulfuric acid solution and measuring the weight change.[17] Our approach to controlling water content was different

* Electrochemical Society Active Member.
[c] Present address: Giner Electrochemical Systems, LLC, Newton, MA 02466, USA.
[z] E-mail: jstaser@ginerinc.com; weidner@cec.sc.edu

than that reported because we controlled the acid concentration rather than the water content of gas in contact with the membrane.[26-29] The catalyst thickness was measured with a thickness gauge by subtracting the membrane thickness from the total MEA thickness. Due to equal catalyst loading at the anode and cathode, the thickness of each catalyst layer was taken to be half the total catalyst thickness.

Model Development

The operating electrolyzer potential, measured at all current densities, is composed of several individual components. Specifically, the electrolyzer potential is the sum of the reversible cell potential U_{eq}, the potential rise due to the ohmic resistance of the membrane iR_A, the cathodic overpotential η_c, and the anodic overpotential, η_a. This may be expressed as

$$V = U_{eq} + iR_A + \eta_c + \eta_a \quad [3]$$

The anodic overpotential can be further divided into an ohmic resistance in the catalyst layer and activation and concentration overpotentials. To adequately predict the electrolyzer potential, we must be able to predict the individual contributions to the total cell potential.

Reversible cell potential.— Water transport influences the sulfuric acid concentration at the anode, which in turn has been shown to affect the reversible potential.[18] A mathematical relationship between the reversible potential for SO_2 oxidation (U_{SO_2}) and the concentration of sulfuric acid produced at the anode is given below based on model results shown previously at $P_{SO_2} = 101$ kPa and $T = 80°C$ [18]

$$U_{SO_2} = 6 \times 10^{-4}[H_2SO_4]^3 - 1.07 \times 10^{-2}[H_2SO_4]^2 + 8.51 \times 10^{-2}[H_2SO_4] + 5.66 \times 10^{-2} \quad [4]$$

where $[H_2SO_4]$ is the concentration of sulfuric acid at the anode in mol/L. The reversible cell potential, in addition to depending on the concentration of sulfuric acid produced at the anode, is a function of the pressure at which hydrogen is produced at the cathode via the Nernst equation

$$U_{H_2} = U^0_{H_2} + \frac{RT}{nF}\ln\frac{P_{H_2}}{P^0_{H_2}} \quad [5]$$

where $U^0_{H_2}$ is the standard potential for the hydrogen electrode and $P^0_{H_2}$ is the standard pressure of the hydrogen electrode (101 kPa). The reversible cell potential is then

$$U_{eq} = U_{SO_2} + U_{H_2} \quad [6]$$

Membrane resistance.— The membrane specific-area resistance (R_A) is a function of the membrane type and thickness and its water content. Several factors influence the membrane water content, including the membrane thickness, temperature, pressure differential, and current density. To determine the membrane water content, we must first determine the water flux across the membrane, which is calculated from the following equation[15-17]

$$N_w = \frac{\rho_M}{M_M\delta_M}\int_{\lambda_a}^{\lambda_c} D_w d\lambda - \frac{\xi\lambda_a i}{\lambda_c F} + \frac{P_M}{\delta_M}(P_c - P_a) \quad [7]$$

The parameters in Eq. 7 have been discussed previously.[15-17] The water content at the cathode (λ_c) is constant and equal to the value for a membrane in contact with liquid water ($\lambda_c = 18$).[15] The water content at the anode (λ_a) depends on the water mole fraction at the anode, which is a function of the water flux[17]

$$y_w = \frac{N_w - \frac{i}{F}}{\left(N_w - \frac{i}{F}\right) + \frac{i}{2F}} \quad [8]$$

where y_w is the mole fraction of water at the anode.[16] Thus[17]

$$\lambda_a = 123.8y_w^3 - 224.01y_w^2 + 134.14y_w - 16.35 \quad [9]$$

This relationship was independent of temperature in the range 50–90°C. Equations 7-9 can be solved simultaneously to give the net water flux in the membrane (N_w) and the water content at the anode (λ_a).

Having calculated N_w from Eq. 7-9, the membrane water content, as a function of position in the membrane, can be obtained by rearranging Eq. 7, such that

$$\frac{d\lambda}{dx} = \frac{M_M\delta_M}{\rho_M}\left[\frac{N_w + \frac{\xi\lambda_a i}{\lambda_c F} - \frac{P_M}{\delta_M}(P_c - P_a)}{D_w}\right] \quad [10]$$

The water distribution in the membrane, solved by integrating Eq. 10 from the cathode to each position in the membrane, is then used to calculate the membrane specific-area resistance by integrating over the local membrane conductivity via the following equation

$$R_A = \int_0^{\delta_M}\frac{dx}{\sigma(\lambda)} \quad [11]$$

where the membrane conductivity σ is a function of the membrane water content λ and is determined experimentally here.

Cathodic overpotential.— The cathodic overpotential of the electrolyzer is due to kinetic losses in the production of hydrogen at the cathode. The electrode resistance has been measured from hydrogen pump experiments by subtracting the resistance of the fully humidified membrane from the measured MEA resistance and dividing that result by 2 (assuming that the ohmic resistance of a like anode and cathode is the same). The result is a linear function of current density

$$i = ai_{0,H_2}L\frac{nF}{RT}\eta_c \quad [12]$$

Anodic overpotential.— The anodic overpotential is a function of three separate components. First, there exists an ohmic resistance in the catalyst layer, which is composed of a liquid phase (i.e., sulfuric acid) and a solid phase (i.e., Pt black). The ohmic contribution is comparable to that measured in the hydrogen pump experiment, which is small.

The final contributions to the anodic overpotential consist of the activation losses and concentration losses. Consider the catalyst layers as porous electrodes in a manner similar to that of Newman and Tobias,[30] with the concentration distribution governed by the competing effects of diffusion and reaction inside the electrode. For the steady-state case described here, the continuity equation becomes

$$D_{SO_2}\frac{d^2C_{SO_2}}{dx^2} - \frac{j_{SO_2}}{nF} = 0 \quad [13]$$

Assuming that the electrochemical reaction obeys Tafel kinetics and is first order in concentration, the reaction rate term in the continuity equation can be represented by

$$\frac{j_{SO_2}}{nF} = \frac{ai_{0,SO_2}}{nF}\left[\frac{C_{SO_2}}{C^0_{SO_2}}\exp\left(\frac{\alpha nF}{RT}\eta_a\right)\right] \quad [14]$$

By making the reasonable assumption that the anodic overpotential (η_a) is constant throughout the catalyst layer, the continuity equation can be reduced to the following form

$$D_{SO_2}\frac{d^2C_{SO_2}}{dx^2} - k^0 C_{SO_2} = 0 \quad [15]$$

where k^0 is a constant represented by

$$k^0 = \frac{ai_{0,SO_2}}{nFC^0_{SO_2}}\exp\left(\frac{\alpha nF}{RT}\eta_a\right) \quad [16]$$

The anodic overpotential is assumed constant throughout the catalyst layer because the conductivities of the solid (i.e., Pt black) and solution (i.e., sulfuric acid solution) phases are high, relative to the kinetic resistance of SO_2 oxidation, resulting in minimal changes in potential with position (i.e., the ohmic resistance is small).

For the case where the free solution interface is at the same side of the catalyst layer as the metal backing, the boundary conditions on the continuity equation can be expressed as

$$C_{SO_2} = C^0_{SO_2} \quad \text{at} \quad x = 0 \quad [17a]$$

$$\frac{dC_{SO_2}}{dx} = 0 \quad \text{at} \quad x = L \quad [17b]$$

and the continuity equation can be solved to render the expression for the concentration profile in the catalyst layer[31]

$$C_{SO_2} = C^0_{SO_2}\frac{\cosh\left[\phi\left(1 - \frac{x}{L}\right)\right]}{\cosh\ \phi} \quad [18]$$

where

$$\phi = \sqrt{\frac{k^0L^2}{D_{SO_2}}} \quad [19]$$

is the Thiele modulus, which relates the rate of reaction to the rate of diffusion in the catalyst layer.

An effectiveness factor (ε) can be defined as the average reaction rate with diffusion divided by the average reaction if the rate of reaction is evaluated at the bulk (or boundary) concentration. Therefore, it can be found by integrating the concentration profile (Eq. 18) throughout the thickness of the catalyst layer to give[31]

$$\varepsilon = \frac{1}{\phi}\tanh\ \phi \quad [20]$$

For small values of the Thiele modulus (ϕ), the effectiveness factor approaches 1, indicating that there are no diffusion limitations and, hence, the catalyst layer is fully utilized. That is, the concentration overpotential is negligible and the activation overpotential dominates. The effectiveness factor decreases as the Thiele modulus increases, indicating that the rate of reaction is affected by the rate of diffusion of the reactant into the catalyst layer.

For electrochemical reactions, the integral of the reaction current throughout the electrode is equal to the applied current. Therefore, the following relationship between the current and the effectiveness factor holds

$$i = \varepsilon La i_{0,SO_2}\ \exp\left(\frac{\alpha nF}{RT}\eta_a\right) \quad [21]$$

Newman and Tobias[30] defined a reaction penetration depth γ as

$$\gamma = \sqrt{\frac{iL}{nFC^0_{SO_2}D_{SO_2}}} \quad [22]$$

This parameter can be combined with the definition of the Thiele modulus and with Eq. 16, 20, and 21 to give

$$\phi = \gamma\sqrt{\frac{\phi}{\tanh\ \phi}} \quad [23]$$

The advantage of introducing γ is that this parameter can be determined from known information. Then, the Thiele modulus (ϕ) and hence the effectiveness factor (ε) can be calculated from the root of Eq. 23 without knowledge of the kinetic parameters. Finally, the effectiveness factor can be used in combination with Eq. 21 to obtain the kinetic parameters from measurements of the applied current vs anodic overpotential.

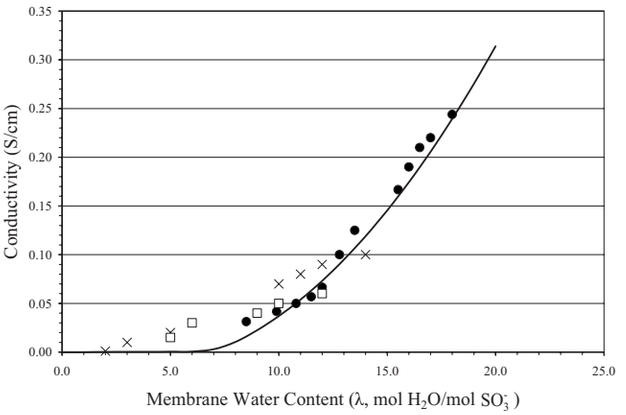

Figure 1. Membrane conductivity as a function of water content. Our data (●) from N115 equilibrated with sulfuric acid at 80°C and the model prediction via Eq. 24 (line) are shown. The other N115 data (×) were equilibrated with humidified air at 80°C.[26] The N117 data (□) were equilibrated with humidified air at 30°C.[27]

Results and Discussion

Membrane resistance.— The membrane conductivity as a function of sulfuric acid concentration was measured via the four-point measurement technique. Combining these data with the water uptake correlation given in Eq. 9 gives the conductivity as a function of water content, which is shown in Fig. 1. The data are for solutions of sulfuric acid concentration ranging from 9 M ($\lambda = 8.5$) to pure water ($\lambda = 18$). The data reported are also shown in Fig. 1 for experiments in which the membrane water content was controlled by the water content of the air in contact with the membrane.[26,27] The following empirical expression has been fitted to our data and is plotted in Fig. 1

$$\sigma = 0.0012\lambda^2 - 0.0083\lambda \quad [24]$$

The greatest mismatch between Eq. 24 and the literature data is at a low water content. However, for the results shown here, the water content of the membrane during electrolyzer operation is above $\lambda = 8$. The water content profile from Eq. 10 is substituted into Eq. 24 and integrated via Eq. 11 to determine the membrane specific-area resistance (R_A). The water content profiles for N212 and N115 at several different current densities, calculated via Eq. 10, are shown in Fig. 2. The water content of the membrane in the HyS electrolyzer decreases from the cathode to the anode due to the sulfuric acid produced at the anode, which effectively reduces the membrane water content.

The specific-area resistances predicted by coupling Eq. 11 and 24 are shown in Fig. 3 for three different membrane thicknesses as a function of current density. The data in Fig. 3 were obtained by the current interrupt technique on working electrolyzers at discrete current densities. Because the current density can be correlated with the net water flux to the anode (and hence sulfuric acid concentration at the anode), the membrane specific-area resistance can be plotted as a function of sulfuric acid concentration produced at the anode, as shown in Fig. 4.

Figure 3 illustrates that the membrane resistance increases with current density. The increase is nearly linear until the electrolyzer reaches high current density, at which point the membrane resistance increases dramatically. For example, the N212 membrane specific-area resistance increases linearly from ~0.02 Ω cm^2 at 0.0 A/cm^2

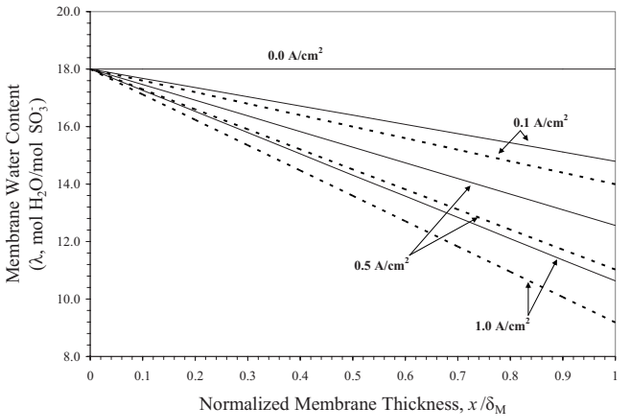

Figure 2. Water content profile of N212 (solid lines) and N115 (dashed lines). The membrane water content decreases from the cathode to the anode due to the sulfuric acid in contact with the anode. The membrane pressure differential was $\Delta P = 600$ kPa and the temperature was 80°C.

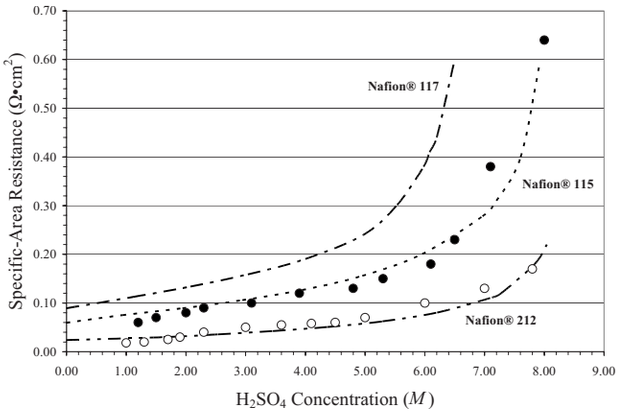

Figure 4. Membrane specific-area resistance as a function of sulfuric acid concentration produced at the anode. The membrane pressure differential was $\Delta P = 600$ kPa and the temperature was 80°C. The points [N212 current interrupt (○) and N115 current interrupt (●)] are experimental data. The lines are model predictions via Eq. 10, 11, and 24.

to 0.095 Ω cm^2 at 0.8 A/cm^2. At current densities higher than 0.8 A/cm^2, however, the membrane specific-area resistance increases much more dramatically. This increase in membrane resistance is due to the increased concentration of sulfuric acid produced at the anode at a high current density. The concentration of sulfuric acid produced at the anode in an N212 electrolyzer operated with a membrane pressure differential $\Delta P = 600$ kPa and at temperature $T = 80$°C at 0.8 A/cm^2 is about 6 M. Examining Fig. 4, the membrane resistance of N212 begins to increase more dramatically at sulfuric acid concentrations above ~6 M. A similar trend is observed for N115 with the same membrane pressure differential and temperature, except that the concentration of sulfuric acid produced at the anode in an N115 electrolyzer reaches 6 M at about 0.5 A/cm^2. Thus, the sharp increase in membrane resistance for N115 is observed at current densities greater than 0.5 A/cm^2 in Fig. 3.

The effect of sulfuric acid concentration produced at the anode on membrane resistance is now understood. As the sulfuric acid concentration produced at the anode increases, the membrane water content decreases. Because the conductivity of Nafion is dependent on membrane water content, a decrease in the water content leads to a decrease in the membrane conductivity. Thus, operating the

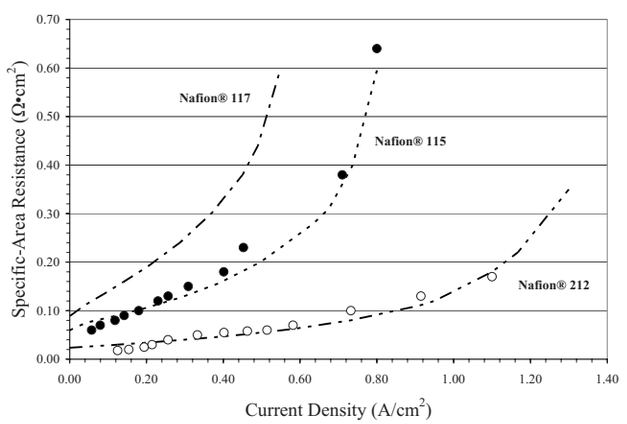

Figure 3. Membrane specific-area resistance as a function of current density. The membrane pressure differential was $\Delta P = 600$ kPa and the temperature was 80°C. The points [N212 current interrupt (○) and N115 current interrupt (●)] are experimental data. The lines are model predictions via Eq. 10, 11, and 24.

Nafion-based electrolyzer at high current densities or with a thick membrane, where a high concentration of sulfuric acid is produced at the anode, increases membrane resistance and results in high cell potential.

Cathodic overpotential.— The cathodic overpotential vs current density is related via Eq. 12. This equation is fitted to the electrode resistance (i.e., half of the difference between the MEA resistance and the membrane resistance from the hydrogen pump data) to give

$$\eta_c = 0.0062i \qquad [25]$$

The electrode resistance of 0.0062 Ω cm^2 is actually the sum of the kinetic and ohmic resistances of the electrode. However, this resistance is small relative to the other resistances in this cell and, therefore, no attempt is made to separate these resistances. The small potential loss due to the resistance of the cathode is consistent with that reported previously for the hydrogen reaction.[32]

Anodic overpotential.— The anodic overpotential can be obtained by subtracting the predicted values of the reversible cell potential, the ohmic resistance of the membrane, and the cathodic overpotential from the measured cell potential. These values are shown in Fig. 5 for N115 at three catalyst loadings and N212 at a catalyst loading of 1.5 mg/cm^2. Also shown in this figure is the fit of Eq. 21 to these data. Because the intrinsic kinetic parameter ai_{0,SO_2} should be the same for all experimental runs, Eq. 21 is fitted to these data to obtain a single value for ai_{0,SO_2} of 1.9×10^{-3} A/cm^3. No attempt has been made to determine either a or i_{0,SO_2} individually. To perform this fit, the diffusion coefficient and solubility of SO_2 in sulfuric acid from the literature was used, and these values are shown in Table I.[33] The SO_2 concentration, $C^0_{SO_2}$, is a function of pressure and temperature and a weak function of sulfuric acid concentration.[18] It was assumed constant at all current densities shown here.

Although all the data in Fig. 5 appear to overlap, there are actually three distinct curves that result when plotting Eq. 21 along with the data. That is, even though $ai_{0,SO_2} = 1.9 \times 10^{-3}$ A/cm^3 is used throughout, the anodic overpotentials at a given current are different for different catalyst loadings. There are two reasons for this dependence, and they work in opposite directions. First, higher catalyst loadings result in lower overpotentials because the reaction occurs over more catalyst sites. However, higher catalyst loadings also correspond to thicker electrodes, which lead to enhanced mass-transfer resistance. The weak dependency of the anodic overpotential on

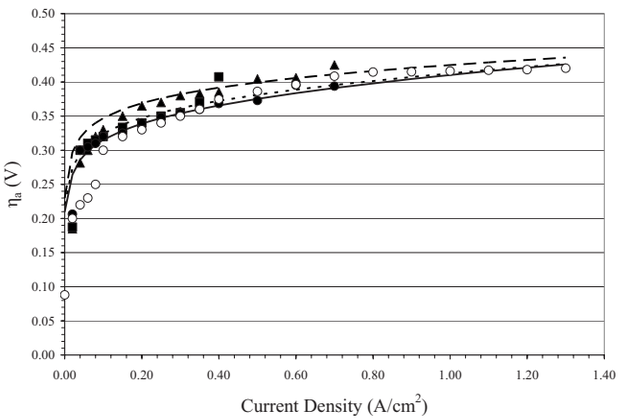

Figure 5. Anodic overpotential for N115 [0.5 mg/cm^2 (▲), 1.0 mg/cm^2 (■), and 1.5 mg/cm^2 (●)] and N212 [1.5 mg/cm^2 (○)]. The lines [0.5 mg/cm^2 (— —), 1.0 mg/cm^2 (- - -), and 1.5 mg/cm^2 (—)] are model predictions via Eq. 21. The membrane pressure differential was ΔP = 600 kPa and the temperature was 80°C.

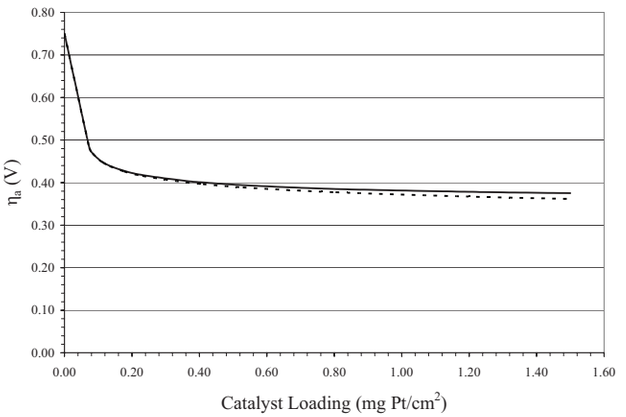

Figure 6. Anodic overpotential as a function of catalyst loading at 0.5 A/cm^2. The solid lines consider mass-transfer limitations, whereas the dotted lines ignore mass transfer. The electrode thickness increases linearly with catalyst loading. There is little effect of catalyst loading on overpotential higher than about 0.2 mg/cm^2. The overpotential increases dramatically, however, at catalyst loadings below 0.1 mg/cm^2.

catalyst loading is consistent with the weak dependency we observed for the total cell potential on catalyst loading.[14]

To understand whether the small dependence of the anodic overpotential on catalyst loading is a result of these two competing effects canceling each other or whether it is simply that each effect is small, the effect of catalyst loading on the anodic overpotential is simulated via Eq. 21 over a wide range of catalyst loadings (i.e., 0.001–1.5 mg/cm^2). These results are plotted in Fig. 6 at a current density of 0.5 A/cm^2 and assuming that the catalyst layer thickness is a linear function of catalyst loading. Also shown in Fig. 6 is Eq. 21 plotted for an effectiveness factor equal to 1.0 at all current densities (i.e., negligible mass-transfer resistance). It is evident from this figure that the concentration overpotential is negligible for loadings less than 1.5 mg/cm^2. Even at this upper value, where the effectiveness factor of the catalyst layer is only 0.68, the potential loss is less than 10 mV. Thus, the anodic overpotential is due mainly to slow oxidation kinetics, with ohmic losses and concentration losses comprising only a negligible fraction of the total.

Also evident from Fig. 6 is that at loadings above 0.2 mg/cm^2, the anodic overpotential is a weak function of loading. This weak dependency is due to the logarithmic form of the kinetic expression given by Eq. 21 (i.e., Tafel kinetics). The logarithmic dependency of the Tafel expression is also the reason the anodic overpotential is very large at catalyst loadings below 0.1 mg/cm^2. Therefore, as long as there is a sufficient amount of catalyst (e.g., 0.2 mg/cm^2), little benefit is gained by adding more catalyst.

Total cell potential.— The total cell potential contributions for a catalyst loading of 1.5 mg/cm^2 have been broken up into their individual components in Fig. 7 and 8. The V-iR_A curves have been calculated by subtracting the iR_A contribution from the total cell potential V in Eq. 3. The model predictions in Fig. 7 and 8 closely follow the experimental data, and the model has been extended to the N117 membrane in Fig. 9.

From the breakdown of the total cell potential shown in Fig. 7 and 8, one can see that the most significant contributions to the total cell potential are the reversible cell potential U_{eq}, the ohmic losses iR_A, and the anodic overpotential η_a. The effect of operating conditions (e.g., system temperature and pressure) on the reversible cell potential has been examined extensively in our previous paper.[18] The ohmic losses could be improved by the use of a membrane whose conductivity is not adversely affected by the concentration of sulfuric acid produced at the anode. The anodic overpotential could be improved by operating at higher cell temperatures and by the use of a more active catalyst toward the oxidation of SO_2. Individually, improvements in any or all of these areas could lead to an improvement in the electrolyzer performance and ultimately higher hydrogen production efficiency in the HyS process.

Table I. Parameter values.

Parameter	Value	Reference
ai_{0,SO_2}	1.9 × 10^{-3} A/cm^3	Fit to Eq. 21
α	0.5	Assumed
$C^0_{SO_2}$	1.55 × 10^{-4} mol/cm^3	18
D_{SO_2}	2.5 × 10^{-5} cm^2/s	33
L (0.5 mg/cm^2)	6.0 × 10^{-4} cm	Measured
L (1.0 mg/cm^2)	1.3 × 10^{-3} cm	Measured
L (1.5 mg/cm^2)	1.8 × 10^{-3} cm	Measured
M_M	1100 g/mol	15
n	2 equiv/mol	Reaction 1
ξ	2.5 mol H_2O/mol H^+	15
ρ_M	1.97 g/cm^3	15

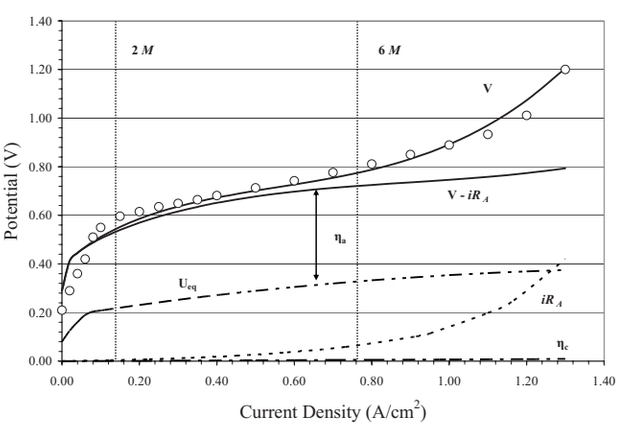

Figure 7. Contributions of the total cell potential for N212. The membrane pressure differential was ΔP = 600 kPa and the temperature was 80°C. The points (○) are experimental data and the lines are model predictions. The total cell potential was predicted as the sum of the individual potential contributions using Eq. 3. The catalyst loading was 1.5 mg/cm^2.

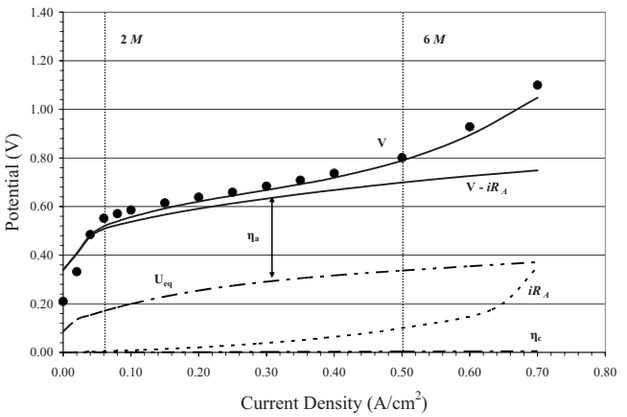

Figure 8. Contributions of the total cell potential for N115. The membrane pressure differential was ΔP = 600 kPa and the temperature was 80°C. The points (●) are experimental data and the lines are model predictions. The total cell potential was predicted as the sum of the individual potential contributions using Eq. 3. The catalyst loading was 1.5 mg/cm^2.

Conclusions

The contributions of reversible cell potential, ohmic losses due to membrane resistance, and anodic overpotential have been investigated for the HyS electrolyzer. The membrane resistance increases with the concentration of sulfuric acid produced at the anode due to the decrease in membrane water content. This dependency is unfortunate because the overall efficiency of the HyS process requires the production of concentrated sulfuric acid in the electrolyzer. Therefore, a membrane in which the conductivity is not adversely affected by concentrated sulfuric acid (i.e., polybenzimidazole[23,34]) may lead to lower total cell potentials. This allows operation at higher current densities (i.e., higher sulfuric acid concentration at the anode), which reduces capital cost and improves efficiency. We have shown that a large anodic overpotential exists, and it is due mainly to activation rather than concentration overpotential. Also, increasing the catalyst loading beyond a minimal value does not significantly improve performance, although the development of more active catalysts toward Reaction 1 may do so. Finally, we have used the model to predict the total cell potential. We have shown the importance of water transport in determining the total cell potential. Water flux to the anode influences the sulfuric acid concentration, which determines the reversible cell potential, the membrane resistance, and the electrode kinetics. Thus, careful control of the membrane water transport is essential for optimized electrolyzer operation for a membrane such as Nafion.

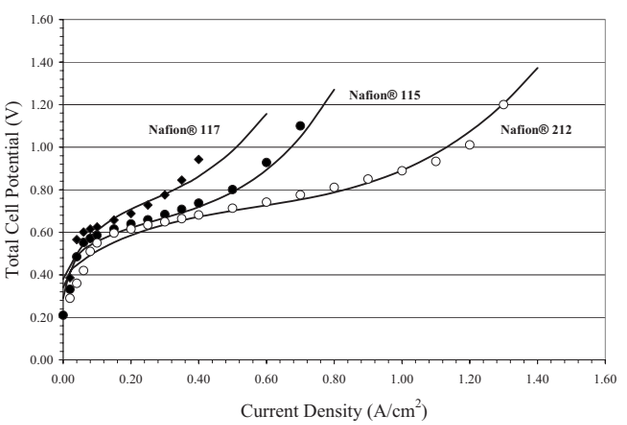

Figure 9. Total cell potential of the HyS electrolyzer as a function of current density and membrane thickness. The model predictions (lines) are composed of the individual contributions (i.e., U_{eq}, iR_A, η_c, and η_a) via Eq. 3. The data [N212 (○), N115 (●), and N117 (♦)] are the polarization data reported previously.[14] The membrane pressure differential ΔP was 600 kPa and the cell temperature was 80°C. The catalyst loading was 1.5 mg/cm^2.

Acknowledgments

This work was partially funded by a Post Academic Career Development grant, SC-INBRE grant no. P20 RR-016461, from the National Center for Research Resources.

University of South Carolina assisted in meeting the publication costs of this article.

List of Symbols

a	specific interfacial area per volume, cm^{-1}
C_{SO_2}	concentration of SO_2 in electrode, mol/cm^3
$C^0_{SO_2}$	bulk concentration of SO_2, mol/cm^3
D_{SO_2}	diffusion coefficient of SO_2 in sulfuric acid, cm^2/s
D_w	diffusion coefficient of water in Nafion, cm^2/s
F	Faraday's constant
i	applied current density, A/cm^2
i_{0,H_2}	exchange current density for the hydrogen evolution reaction, A/cm^2
i_{0,SO_2}	exchange current density for the SO_2 oxidation reaction, A/cm^2
j	electrochemical reaction rate, A/cm^3
k^0	kinetic constant for Reaction 1, s^{-1}
L	catalyst layer thickness, cm
M_M	molecular weight of membrane, g/mol
n	number of electrons transferred
N_w	flux of water through Nafion, mol/cm^2 s
P_k	pressure in region k, kPa
P_M	membrane permeability, mol/(cm s kPa)
R	ideal gas constant
R_A	membrane specific-area resistance, Ω cm^2
T	temperature, K
U_{eq}	reversible cell potential, V
U_{H_2}	potential of the hydrogen electrode, V
$U^0_{H_2}$	standard potential of the hydrogen electrode, V
U_{SO_2}	potential of the SO_2 electrode, V
$U^0_{SO_2}$	standard potential of the SO_2 electrode, V
V	total cell potential, V
x	distance into the electrode, cm
y_w	water mole fraction at anode

Greek

α	transfer coefficient
γ	reaction penetration depth
δ_M	thickness of catalyst coated membrane, cm
ΔP	pressure differential across the membrane ($P_c - P_a$), kPa
ε	effectiveness factor
η_k	overpotential for electrode k, V
λ	water content of the membrane, mol H_2O/mol SO_3^-
λ_k	water content of the membrane at interface k, mol H_2O/mol SO_3^-
ξ	electro-osmotic drag coefficient, H_2O/H^+
ρ_M	density of Nafion, g/cm^3
σ	membrane conductivity, S/cm
ϕ	Thiele modulus

Subscripts

a	anode
c	cathode

References

1. M. B. Gorensek, W. A. Summers, C. O. Bolthrunis, E. J. Lahoda, D. T. Allen, and R. Greyvenstein, "Hybrid Sulfur Process Reference Design and Cost Analysis," Savannah River National Laboratory, Report no. SRNL-L1200–2008–00002, June 12, 2009, http://dx.doi.org/10.2172/956960.
2. Department of Energy (DOE) Energy Information Administration, Hydrogen Use, Petroleum Consumption and Carbon Dioxide Emissions, Washington, DC (2008).
3. E. Varkaraki, N. Lymberopoulos, E. Zoulias, D. Guichardot, and G. Poli, *Int. J. Hydrogen Energy*, **32**, 1589 (2007).
4. Y. Shin, W. Park, J. Chang, and J. Park, *Int. J. Hydrogen Energy*, **32**, 1486 (2007).
5. J. S. Herring, J. E. O'Brien, C. M. Stoots, G. L. Hawkes, J. J. Hartvigsen, and M. Shahnam, *Int. J. Hydrogen Energy*, **32**, 440 (2007).
6. Nuclear Hydrogen R&D Plan Draft, Department Of Energy, Office of Nuclear

Energy, Science and Technology (2004).
7. Nuclear Hydrogen Initiative: Ten Year Program Plan, Office of Advanced Nuclear Research, DOE Office of Nuclear Energy, Science and Technology, March 2005.
8. A. Hauch, S. H. Jensen, S. Ramousse, and M. Mogensen, *J. Electrochem. Soc.*, **153**, A1741 (2006).
9. P. W. Lu, E. R. Garcia, and R. L. Ammon, *J. Appl. Electrochem.*, **11**, 347 (1981).
10. P. W. Lu and R. L. Ammon, *J. Electrochem. Soc.*, **127**, 2610 (1980).
11. P. Sivasubramanian, R. P. Ramasamy, F. J. Freire, C. E. Holland, and J. W. Weidner, *Int. J. Hydrogen Energy*, **32**, 463 (2007).
12. M. B. Gorensek and W. A. Summers, *Int. J. Hydrogen Energy*, **34**, 4097 (2009).
13. F. Jomard, J. P. Feraud, and J. P. Caire, *Int. J. Hydrogen Energy*, **33**, 1142 (2008).
14. J. Staser, R. P. Ramasamy, P. Sivasubramanian, and J. W. Weidner, *Electrochem. Solid-State Lett.*, **10**, E17 (2007).
15. J. A. Staser and J. W. Weidner, *J. Electrochem. Soc.*, **156**, B16 (2009).
16. J. A. Staser, K. Norman, C. H. Fujimoto, M. A. Hickner, and J. W. Weidner, *J. Electrochem. Soc.*, **156**, B842 (2009).
17. J. A. Staser and J. W. Weidner, *J. Electrochem. Soc.*, **156**, B836 (2009).
18. M. B. Gorensek, J. A. Staser, T. G. Stanford, and J. W. Weidner, *Int. J. Hydrogen Energy*, **34**, 6089 (2009).
19. S.-K. Lee, C.-H. Kim, W.-C. Cho, K.-S. Kang, C.-S. Park, and K.-K. Bae, *Int. J. Hydrogen Energy*, **34**, 4701 (2009).
20. B. S. Pivovar and Y. S. Kim, *J. Electrochem. Soc.*, **154**, B739 (2007).
21. *Springer Handbook of Electronic and Photonic Materials*, S. Kasap and P. Capper, Editors, pp. 410–413, Springer Science+Business Media, New York (2006).
22. Y.-L. Ma, J. S. Wainright, M. H. Litt, and R. F. Savinell, *J. Electrochem. Soc.*, **151**, A8 (2004).
23. J. S. Wainright, J. T. Wang, R. F. Savinell, and M. H. Litt, *J. Electrochem. Soc.*, **142**, L121 (1995).
24. B. D. Cahan and J. S. Wainright, *J. Electrochem. Soc.*, **140**, L185 (1993).
25. X. Ye and C.-Y. Wang, *J. Electrochem. Soc.*, **154**, B676 (2007).
26. C. Yang, S. Srinivasan, A. B. Bocarsly, S. Tulyani, and J. B. Benziger, *J. Membr. Sci.*, **237**, 145 (2004).
27. T. A. Zawodzinski, Jr., C. Derouin, S. Radzinski, R. J. Sherman, V. T. Smith, T. E. Springer, and S. Gottesfeld, *J. Electrochem. Soc.*, **140**, 1041 (1993).
28. S. Slade, S. A. Campbell, T. R. Ralph, and F. C. Walsh, *J. Electrochem. Soc.*, **149**, A1556 (2002).
29. R. F. Silva, M. De Francesco, and A. Pozio, *J. Power Sources*, **134**, 18 (2004).
30. J. S. Newman and C. W. Tobias, *J. Electrochem. Soc.*, **109**, 1183 (1962).
31. B. A. Finlayson, *Nonlinear Analysis in Chemical Engineering*, McGraw-Hill Chemical Engineering Series, New York (1980).
32. K. C. Neyerlin, W. Gu, J. Jorne, and H. A. Gasteiger, *J. Electrochem. Soc.*, **154**, B631 (2007).
33. D. G. Leaist, *J. Chem. Eng. Data*, **29**, 281 (1984).
34. J. Mader, L. Xiao, T. J. Schmidt, and B. C. Benicewicz, *Adv. Polym. Sci.*, **216**, 63 (2008).